



Solid solution $Pb_{1-x}Eu_xTe$: constitution and thermoelectric behavior

Journal:	<i>Inorganic Chemistry Frontiers</i>
Manuscript ID	QI-RES-05-2016-000161.R1
Article Type:	Research article
Date Submitted by the Author:	28-Jun-2016
Complete List of Authors:	Wang, Xin-Ke; Max-Planck-Institut fur Chemische Physik fester Stoffe, Chemische Metallkunde Veremchuk, Igor; Max-Planck-Institut fur Chemische Physik fester Stoffe Bobnar, Matej; MPI CPfS, Chemical Metals Science Zhao, Jing-Tai; Shanghai University, Electronic Information Materials Grin, Yuri; MPI CPfS, Chemical Metals Science

Solid solution $\text{Pb}_{1-x}\text{Eu}_x\text{Te}$: constitution and thermoelectric behaviorXin-Ke Wang¹, Igor Veremchuk¹, Matej Bobnar¹, Jing-Tai Zhao^{2*}, Yuri Grin^{1*}¹ *Max-Planck-Institut für Chemische Physik fester Stoffe, 01187 Dresden, Germany*² *School of Materials Science and Engineering, Shanghai University, Shanghai 200444, China***Abstract**

Polycrystalline samples of the solid solution $\text{Pb}_{1-x}\text{Eu}_x\text{Te}$ were prepared by the spark-plasma technique. In contrast to literature data, the homogeneity range of the solid solution amounts only to $0 \leq x \leq 0.02$ at the selected preparation conditions. The implementation of Eu into the PbTe lattice was monitored by refinement of the lattice parameters. Thermoelectric properties of the prepared materials were investigated above room temperature. In samples with compositions $x \leq 0.04$, the solid solution $\text{Pb}_{1-x}\text{Eu}_x\text{Te}$ reveals a metal-semiconductor transition around 500 K going in parallel to the p - n transition in the conductivity. No significant influence of the europium substitution on the thermoelectric figure-of-merit was observed in stoichiometric bulk materials.

Keywords: PbTe; Eu-substitution; solid solution; p - n transition; thermoelectric properties.

*Correspondence authors: grin@cpfs.mpg.de; jtzhao@shu.edu.cn

1. Introduction

With low thermal conductivity and suitable electronic transport properties, the semiconductor lead telluride is one of leading thermoelectric materials in the mid-temperature range^{1,2}. In 1959, the first radioisotope thermoelectric generator (RTG) contained both *n*- and *p*-type PbTe materials to convert radioisotope heat to electricity^{3,4}. For over half a century PbTe-based thermoelectrics have successfully provided power on various NASA's missions⁵⁻⁷. Scientific reports on these materials started to appear in the literature in the 1950s and 1960s, and in the following period a vast amount of experimental data were gathered on PbTe-based materials for thermoelectric applications⁸⁻¹³. Measurements of the temperature dependence of the Hall coefficient and the electrical resistivity have been presented for *p*-type PbTe yielding a carrier concentration range from 10^{17} to 10^{20} cm⁻³^{9,10}. An effective two-valence band model of PbTe was proposed in 1966 by Allgaier and Houston¹¹ and confirmed in 1967 by Crocker and Rogers¹⁴. Those works are mainly based on single crystals grown by the Bridgman technique, and only a few publications report on the electrical and thermal transport properties of polycrystalline binary PbTe¹⁵⁻¹⁷. Some controversies still exist concerning the basic understanding of the origin of low lattice-thermal conductivity of lead telluride¹⁸⁻²⁰.

To enhance the thermoelectric performance of PbTe, series of studies utilizing electron and phonon engineering approaches were performed on chemically substituted materials,²². So far, sodium and iodine have been proven to be the best dopants yielding *p*- and *n*-type PbTe-based materials, respectively^{4,21,23}. Specific changes of the electronic density of states by TI-substitution in PbTe result in an enhancement of *ZT* to above 1.5 at 773 K²⁴. In general, a material with a delta-shaped density of states around the Fermi level is believed to have an enhanced *ZT*²⁵, and

nanostructuring is an effective way to enhance the thermoelectric potential of lead telluride²⁶⁻²⁸.

Largely enhanced thermoelectric figures-of-merit at room temperature (RT) have been theoretically predicted for quantum wells $\text{Pb}_{1-x}\text{Eu}_x\text{Te}$ and confirmed experimentally for thin films²⁹⁻³². Samples of the pseudo-binary system $\text{PbTe-Eu}_2\text{Te}_3$ with low concentration (less than 5.0 mol %) of Eu_2Te_3 showed - with increasing Eu content – a decrease of the thermal conductivity combined with the opposite tendencies in the changes of electrical conductivity and Seebeck coefficient (maximal Seebeck coefficient of 315 mV K^{-1} and minimal conductivity of $22.5 \times 10^{-3} \text{ S m}^{-1}$ at 1 mol % of Eu_2Te_3 , all properties were measured at RT)³³. The composition of the samples studied in Ref. 33 are not exactly within the solid solution $\text{Pb}_{1-x}\text{Eu}_x\text{Te}$. No changes in the charge carrier concentration were found in the presence of europium in the chemically analogous system $\text{Pb}_{1-x}\text{Eu}_x\text{Se}$ ³⁴.

According to the phase diagram of the Eu-Te system³⁵, the equiatomic phase has a homogeneity range between 50 and 57 at % of Te. This would mean a partial presence of europium in the f^6 (Eu^{3+}) state. Under such circumstances, a substitution of Pb in PbTe by europium may strongly influence the electronic density of states at the Fermi level and, consequently, the electronic transport properties relevant for thermoelectric behaviour.

In order to investigate these different possibilities to influence the thermoelectric properties of lead telluride, we report herein on the constitution as well as on the thermoelectric and the carrier-transport properties of the polycrystalline solid solution $\text{Pb}_{1-x}\text{Eu}_x\text{Te}$ above RT.

2. Experimental details

Polycrystalline samples $\text{Pb}_{1-x}\text{Eu}_x\text{Te}$ with x of 0, 0.005, 0.010, 0.015, 0.020, 0.030, 0.040, 0.050, 0.100 and 0.500 were synthesized by melting the elements Pb (shot, 99.999 mass %), Te (chunk, 99.9999 mass %), Eu (chunk, 99.95 mass %) in a graphite-coated and fused silica tube at 1273 K for 6 h under a pressure of around 10^{-4} torr, before cooling down within one hour to 873 K and holding there for six days for homogenization. The obtained ingots were ground into powders by hand using an agate mortar in argon atmosphere before spark-plasma sintering (Fuji SPS-515S) at 673 K under a pressure of 60 MPa for 7 minutes. The SPS-prepared disks ($\varnothing = 10$ mm, 2 mm thick) were polished for measurements of the thermal diffusivity (LFA). After the measurement, the disks were cut into rectangular blocks ($2 \times 2 \times 8$ mm³) in order to measure electrical resistivity and Seebeck coefficient (ZEM-3 setup).

Phase identification was performed with the X-ray Guinier diffraction technique (Huber G670 camera, Cu $K_{\alpha 1}$ radiation, $\lambda = 1.54056$ Å, $\Delta 2\theta = 0.005^\circ$, 2θ range 3.0° - 100° , exposure time 6×15 min). The reflection positions obtained by profile deconvolution were corrected using the internal standard LaB_6 . Lattice parameter refinement and other crystallographic calculations were performed with the program package WinCSD³⁶.

The in-situ high-temperature powder X-ray diffraction experiments were performed at the ID22 beamline of the ESRF, Grenoble (multi-channel detector, $2\theta_{\text{max}} = 28.5^\circ$, $\Delta 2\theta = 0.002^\circ$, $\lambda = 0.354337(3)$ Å). The sample powder was loaded into quartz capillaries with 0.3 mm diameter. The hot-air blower was used for generating of temperatures up to 500 °C.

For the metallographic study, the sample pieces were embedded in conductive resin, subsequently grinded and polished. The microstructures of the samples were analyzed using optical (including polarized light) and electron microscopy. The

back-scattered electron (BSE) micrographs and energy dispersive X-ray spectroscopy (EDXS) analyses were made on a Philips XL30 scanning electron microscope with attached silicon drift detector (Bruker Quantax 400 system with the detector XFlash 630). Elemental chemical analysis (for Pb, Te, Eu, O, C, Si, Al) was performed on samples after SPS (around 100 mg) by using the inductively-coupled plasma optical-emission spectrometry (ICP-OES, Agilent 5100 SVDV setup for Pb, Te, Eu, Si, Al) and the carrier-gas hot-extraction technique (LECO C200 setup for carbon and LECO TCH600 setup for oxygen).

Thermal gravimetry (TG) and differential scanning calorimetry (DSC) were performed employing the Netzsch STA 449C and Netzsch DSC 404C. The measurement of TG was made with a heating rate of 5 K min^{-1} between room temperature and 773 K in an open graphite crucible. Then the sample was kept for 12 hours in argon. The DSC was made between room temperature and 1248 K with a heating rate of 5 K min^{-1} .

Electrical resistivity and Seebeck coefficient were measured simultaneously with the ZEM-3 setup (Ulvac-Riko) in the temperature range 300 to 673 K. Thermal diffusivity (D) was conducted with the Netzsch LFA 457 equipment. The Hall effect (R_H) was measured with a standard six-point ac technique in a physical property measurement system (PPMS, Quantum Design), with magnetic fields up to 9 T. The Hall carrier concentrations were calculated by $1/(R_H \cdot e)$, R_H is Hall coefficient, e is the charge of an electron. The heat capacity per atom (C_p) was estimated from the relation $C_p/k_B = 3.07 + 0.00047(T - 300)$ (Ref. 37). Thermal conductivity was calculated as $\kappa = dC_pD$, where d is the density obtained using the mass and geometric volume of the specimen disk. Lattice thermal conductivity (κ_L) was calculated by subtracting the

electronic part $\kappa_e = L\sigma T$ ($L = 2.44 \times 10^{-8} \text{ W} \cdot \Omega \cdot \text{K}^{-2}$ is the Lorenz number and σ is the electrical conductivity) from the total conductivity.

3. Results and discussions

In some earlier publications the equiatomic phase in the system Pb-Te was reported to exhibit a homogeneity range^{38,39}. Fig. 1a presents the powder XRD patterns of synthesized samples with different Pb:Te atomic ratio around the equiatomic composition. All prepared binary samples have the same lattice parameters within two to three estimated standard deviations. Moreover, only stoichiometric samples $\text{Pb}_{50}\text{Te}_{50}$ show single phase behavior while other samples contain minority phases (elements Pb or Te). Metallographic investigation in polarized light (Fig. 1b) and element mapping of the sample $\text{Pb}_{50}\text{Te}_{50}$ confirm the presence of a homogenous single-phase material. The total composition for this sample is 49.83 ± 0.20 at % Pb and 50.17 ± 0.20 at % Te according to the chemical analysis; no other elements (analyzed elements: Pb, Te, Si, O, C) were found. These findings indicate that the phase PbTe has either a point composition or a very narrow homogeneity range. This result is in good agreement with more recent literature data⁴⁰⁻⁴².

The phases PbTe and EuTe crystallize both in the NaCl structure type, and it is commonly assumed that they form a solid solution over the entire concentration range $\text{Pb}_{1-x}\text{Eu}_x\text{Te}$. However, the lattice parameters increase nonlinearly and do not obey Vegard's relation⁴³⁻⁴⁶. In order to verify that, samples $\text{Pb}_{1-x}\text{Eu}_x\text{Te}$ with $0.005 \leq x \leq 0.04$ were used. The lattice parameter of the $\text{Pb}_{1-x}\text{Eu}_x\text{Te}$ phase changes linearly with the composition for $x \leq 0.02$, and then remains unchanged. The slight reduction of the lattice parameter for the same composition after SPS is most probably caused by

homogenization of the materials during spark-plasma treatment. The X-ray powder diffraction patterns of samples with $x \geq 0.03$ contain reflections of the cubic phases $\text{Pb}_{1-x}\text{Eu}_x\text{Te}$ and $\text{Eu}_{1-x}\text{Pb}_x\text{Te}$ (Fig. 2b). The microstructure analysis confirms the single-phase character of the samples with $x \leq 0.02$ (Fig. 3c). Thus, europium has only limited solubility in PbTe. This finding is in disagreement with Ref. 44. An attempt to apply the preparation technique used in Ref. 44 (heating of components in arc-welded tantalum crucibles at 1223 K for seven days) was not successful: the sample with $x = 0.50$ clearly comprised two phases. The same result was achieved by induction heating to the melt (Fig. 2b). The obtained limit concentration of europium ($x \leq 0.02$) is in better agreement with the phase diagram²¹ showing substitutional solid solution with about 5 at % Eu in PbTe at room temperature, and is in contrast to the results of Ref. 44.

The electrical resistivity of samples $\text{Pb}_{1-x}\text{Eu}_x\text{Te}$ shows a bad-metal behavior in the low-temperature range below 500 K, and then changes to a semiconducting characteristic at higher temperatures (Fig. 4a), similarly to the binary compound^{10,14,51,52}. The Seebeck coefficient changes sign in the same temperature range indicating a p - n transition (Fig. 4b). The thermal conductivity decreases with temperature below the p - n transition and remains practically unchanged above the transition (Fig. 4c, d). With increasing europium content, the resistivity around room temperature first decreases to $x = 0.01$ and then increases toward $x = 0.04$ (Fig. 4a). Taking into account that the samples with $x \geq 0.02$ contain small amounts of the minority phases and considering an additional scattering effect of point defects of the second phase, the resistivity increase may be caused by a microstructure effect. The Seebeck coefficient changes slightly with x and behaves similarly to the resistivity, in particular around room temperature (Fig. 4b, insert). The thermal conductivity shows

the opposite tendency. Upon substitution, it first slightly increases before it decreases with x (Fig. 4c, d).

Electrical resistivity and Seebeck coefficient keep stable for several measurement cycles (Fig. 5). This shows that the materials are sufficiently homogenous and do not change with the exposition time. Such behavior does not depend on the europium concentration.

In order to exclude a structural transition as potential reason for the non-monotonic behavior of thermoelectric properties, high-temperature X-ray diffraction experiments were carried out. The temperature dependence of the lattice parameter for $\text{Pb}_{50}\text{Te}_{50}$ shows linear behavior which can be described by the equation $a(T) = 6.4206 + 1.4 \times 10^{-4}T$ (Fig. 6a). The linear thermal expansion coefficient at room temperature amounts to $2.17 \times 10^{-5} \text{ K}^{-1}$, which is in good agreement with literature values determined by capacitance⁴⁷ and X-ray diffraction¹⁹. No structural transition is observed around 500 K.

According to thermogravimetric analysis, lead telluride $\text{Pb}_{50}\text{Te}_{50}$ starts to decompose at 773 K and loses about 0.9 mass % just after 12 hours at this temperature in an open graphite crucible under argon atmosphere (Fig. 6b). Similar behavior was observed in other studies^{48, 49}, ascribed to components' sublimation. The latter should be responsible for the weak mechanical strength at high temperature⁵⁰. Annealing the sample in vacuum at 773 K for one day yields lots of voids (Fig. 3a) which appear near the grain boundaries. The chemical analysis shows 49.76 ± 0.10 at % Pb; the Pb:Te ratio does not change after annealing. Thermal analysis did not yield any hint at a structural transformation: DSC (differential scanning calorimetry) measurements reveal only one exothermic peak at 1180 K (Fig. 6c), reflecting the melting point of PbTe well in agreement with the phase diagram⁴².

The powder XRD patterns of $\text{Pb}_{50}\text{Te}_{50}$ after SPS preparation reveal unusual peak broadening (Fig. 7). At temperatures below 473 K, a strong anisotropy of the reflection broadening is observed: the $h00$ peaks show much lower full width at half maximum in comparison to the $hk0$ and hkl ones. This anisotropy reduces strongly in the range between 473 K and 573 K and is practically not more observed above 573 K. Moreover, the reflection broadening in general reduces with the increasing temperature. The temperature range, where the anisotropy of the reflection broadening for $\text{Pb}_{50}\text{Te}_{50}$ diminishes, correlates with the strong change in the electronic and thermal transport behavior of the binary material and the solid solution $\text{Pb}_{1-x}\text{Eu}_x\text{Te}$.

Transport properties, which are very similar to those observed in the present study, were reported for single crystals of PbTe with low charge carrier concentrations (10^{17} - 10^{18} cm^{-3})^{10,14,51,52}, and they also have been theoretically described by a three-band model calculation⁵³. Hall effect measurements for $\text{Pb}_{1-x}\text{Eu}_x\text{Te}$ yield hole concentrations between 3×10^{17} and 11×10^{17} cm^{-3} at room temperature depending on x , being thus of the same order of magnitude. Since no phase transition and no chemical composition change¹⁰ occurs, the non-monotonic behavior of the transport properties can be explained by lattice defects in PbTe. The study of the composition limits suggests that the predominant atomic point defects are Pb vacancies (V_{Pb}) and Te vacancies (V_{Te}), cf Ref. 54. A photoreflectance (PR) spectrum of PbTe shows that there are three energy transitions which may relate to V_{Pb} , V_{Te} , see Ref. 55. The higher formation energy of Frenkel defects indicates that the diffusion is essentially controlled by a vacancy-type mechanism¹⁰. According to first principles density functional theory (DFT), V_{Pb} and V_{Te} have the lowest formation energies in the PbTe binary system⁵⁶. Both vacancies exist in the samples (so-called Schottky defects). The V_{Te} form a deeply located defect state in the band

gap, the V_{Pb} generate a shallow state near the maximum of valence band⁵⁷. Therefore, at low temperature, V_{Pb} acts as acceptor and the samples are p -type conductors with “extrinsic” conduction behavior. With increasing temperature, V_{Te} are activated and contribute electrons to the conduction band so that the samples begin move into the range of “intrinsic” conduction, which causes the metal-semiconductor transition in the electrical conductivity around 500 K. According to the relation between the number of intrinsic electrons n_i and the energy gap ΔE and relating the Hall constant R_H and the conductivity σ with the concentration of conduction electrons and holes n , p under consideration of the mobility of electrons and holes μ_n , μ_p , the fit the experimental data of R_H , σ and optical value of ΔE yields the mobility ratio $b = \mu_n/\mu_p$ ⁸. Similar methods performed on the Hall coefficient data give the same results^{6,58}: the electron mobility is much higher than the hole mobility at temperatures above 300 K, and the mobility ratio increases to 2.5 above 400 K. This is mainly attributed to the heavy second valence band becoming dominant for the hole transport above 400 K causing a significant reduction of the average hole mobility¹². With higher concentration and mobility, the electrons will dominate the conduction behavior when crossing a certain temperature. Intrinsic excitation based on the energy band gap at elevated temperature will accelerate the transition. Due to the obvious similarity of the temperature dependences of properties between the ternary materials and the binary PbTe, we assume the same or at least a similar mechanism causing this behaviour.

The thermoelectric figure-of-merit ZT values for $Pb_{1-x}Eu_xTe$ samples are in same range (Fig. 8) and have maximal values in the temperature range below the p - n transition due to the high Seebeck coefficient and the improved conductivity.

Lead-by-europium substitution does not influence the thermoelectric ability of stoichiometric lead telluride strongly.

4. Conclusions

Samples in and around the pseudo-binary section $\text{Pb}_{1-x}\text{Eu}_x\text{Te}$ of the ternary system $\text{Pb}-\text{Eu}-\text{Te}$ were synthesized for $0.00 \leq x \leq 0.50$. The substitutional solid solution of europium in PbTe is markedly lower than that reported before in the literature. The thermoelectric properties of the prepared materials $\text{Pb}_{1-x}\text{Eu}_x\text{Te}$ with different europium content were systematically measured in the temperature range between 300 and 673 K. The solid solution $\text{Pb}_{1-x}\text{Eu}_x\text{Te}$ undergoes a metal-semiconductor transition in parallel to the $p-n$ transition in the conductivity around 500 K. No evidence for a structural transformation was found, neither by high-temperature synchrotron powder diffraction nor by differential scanning calorimetry and thermogravimetric analysis. The electron transport behavior of binary PbTe is in agreement with the intrinsic point defects mechanism. Lead-by-europium substitution causes systematical changes of resistivity, Seebeck coefficient and thermal conductivity which can be understood in terms of an isoelectronic substitution, i.e. europium remains in the f^7 (Eu^{2+}) state. Consequently, no significant influence of this substitution on the thermoelectric figure-of-merit was observed in bulk stoichiometric PbTe . This finding is in sharp contrast to the behavior of thin films as reported in the literature.

Acknowledgements

Authors thank Dr. Yurii Prots (MPI CPfS) and Dr. Yves Watier (ESRF) for assistance with synchrotron measurements, Dr. Ulrich Burkhardt (MPI CPfS) for support in

metallographic investigations, Dr. Marcus Schmidt (MPI CPfS) for DSC-TG measurements, Dr. Gudrun Auffermann (MPI CPfS) for chemical analysis, and Dr. Ulrich Schwarz (MPI CPfS) for valuable discussions.

A part of this work was performed within the MOU between the MPI CPfS and the Shanghai University.

References

1. O. Delaire, J. Ma, K. Marty, A. F. May, M. A. McGuire, M. H. Du, D. J. Singh, A. Podlesnyak, G. Ehlers, M. D. Lumsden and B. C. Sales, *Nat. Mater.*, 2011, **10**, 614-619.
2. A. D. LaLonde, Y. Pei, H. Wang and G. J. Snyder, *Mater. Today*, 2011, **14**, 526-532.
3. H. Zhu, W. Sun, R. Armiento, P. Lazic and G. Ceder, *Appl. Phys. Lett.*, 2014, **104**, 082107.
4. Y. Z. Pei, A. LaLonde, S. Iwanaga and G. J. Snyder, *Energy Environ. Sci.*, 2011, **4**, 2085-2089.
5. C. Wood, *Rep. Prog. Phys.*, 1988, **51**, 459-539.
6. Y. I. Ravich, B. A. Efimova and I. A. Smirnov, *Semiconducting Lead Chalcogenides*, Plenum Press, 1970, 330-334.
7. D. M. Rowe, *Thermoelectrics Handbook: Macro to Nano*, CRC Press 2006.
8. R. A. Smith, *Physica*, 1954, **20**, 910-929.
9. R. S. Allgaier and W. W. Scanlon, *Phys. Rev.*, 1958, **111**, 1029-1037.
10. E. Miller, K. Komarek and I. Cadoff, *J. Appl. Phys.*, 1961, **32**, 2457-2465.
11. R. S. Allgaier and B. B. Houston, *J. Appl. Phys.*, 1966, **37**, 302-309.
12. R. N. Tauber, A. A. Machonis and I. B. Cadoff, *J. Appl. Phys.*, 1966, **37**, 4855-4860.
13. R. Dalven, *Infrared Physics*, 1969, **9**, 141-184.
14. A. J. Crocker and L. M. Rogers, *Brit. J. Appl. Phys.*, 1967, **18**, 563-572.
15. S. Yoneda, E. Ohta, H. T. Kaibe, I. J. Ohsugi, I. Shiota and I. A. Nishida, *Mat. Trans. Jap. Inst. Mater.*, 2001, **42**, 329-335.
16. Y.-L. Pei and Y. Liu, *J. Alloys Compd.*, 2012, **514**, 40-44.
17. R. Breschi, A. Olivi, A. Camanzi and V. Fano, *J. Mater. Sci.*, 1980, **15**, 918-924.
18. E. S. Bozin, C. D. Malliakas, P. Souvatzis, T. Proffen, N. A. Spaldin, M. G. Kanatzidis and S. J. L. Billinge, *Science*, 2010, **330**, 1660-1663.
19. S. Kastbjerg, N. Bindzus, M. Sondergaard, S. Johnsen, N. Lock, M. Christensen, M. Takata, M. A. Spackman and B. B. Iversen, *Adv. Funct. Mater.*, 2013, **23**, 5477-5483.
20. T. Keiber, F. Bridges and B. C. Sales, *Phys. Rev. Lett.*, 2013, **111**, 95504.
21. S. Ahmad, S. D. Mahanti, K. Hoang and M. G. Kanatzidis, *Phys. Rev. B*, 2006, **74**, 155205.
22. S. Paschen, C. Godart, Yu. Grin, In: *Complex Metallic Alloys: Fundamentals and Applications*, WILEY-VCH, 2011, 365-384.
23. A. D. LaLonde, Y. Z. Pei and G. J. Snyder, *Energy Environ. Sci.*, 2011, **4**, 2090-2096.
24. J. P. Heremans, V. Jovovic, E. S. Toberer, A. Saramat, K. Kurosaki, A. Charoenphakdee, S. Yamanaka and G. J. Snyder, *Science*, 2008, **321**, 554-557.
25. G. D. Mahan and J. O. Sofo, *Proc. Natl. Acad. Sci. USA*, 1996, **93**, 7436-7439.
26. C. J. Vineis, A. Shakouri, A. Majumdar and M. G. Kanatzidis, *Adv. Mater.*, 2010, **22**, 3970-3980.
27. M. Ohta, K. Biswas, S.-H. Lo, J. He, D. Y. Chung, V. P. Dravid and M. G. Kanatzidis, *Adv. Energy Mater.*, 2012, **2**, 1117-1123.
28. K. Biswas, J. Q. He, I. D. Blum, C. I. Wu, T. P. Hogan, D. N. Seidman, V. P. Dravid and M. G. Kanatzidis, *Nature*, 2012, **489**, 414-418.

29. T. C. Harman, D. L. Spears and M. J. Manfra, *J. Electron. Mater.*, 1996, **25**, 1121-1127.
30. A. Casian, I. Sur, H. Scherrer and Z. Dashevsky, *Phys. Rev. B*, 2000, **61**, 15965-15974.
31. I. Sur, A. Casian and A. Balandin, *Phys. Rev. B*, 2004, **69**, 35306.
32. A. Ishida, T. Yamada, D. Cao, Y. Inoue, M. Veis and T. Kita, *J. Appl. Phys.*, 2009, **106**, 23718.
33. I. O. Nasibov, T. I. Sultanov, V. K. Valiev and S. M. Alidzhanova, *Inorganic Materials, translated from Izvestiya Akademii Nauk SSSR, Neorganicheskie Materialy*, 1987, **23**, 457-458.
34. V. Jovovic, S. J. Thiagarajan, J. West, J. P. Heremans, T. Story, Z. Golacki, W. Paszkowicz and V. Osinniy, *J. Appl. Phys.*, 2007, **102**, 43707.
35. O. A. Sadvokskaya, E. I. Yarembash. *Russ. Inorg. Mater., translated from Izvestiya Akademii Nauk SSSR, Neorganicheskie Materialy*, 1970, **6**, 1097-1101.
36. L. Akselrud and Y. Grin, *J. Appl. Crystallogr.*, 2014, **47**, 803-805.
37. Y. Pei, A. D. LaLonde, H. Wang and G. J. Snyder, *Energy Environ. Sci.*, 2012, **5**, 7963-7969.
38. E. Miller, K. Komarek, *Trans. AIME*, 1959, **215**, 882-887.
39. W. Lugscheider, H. Ebel, G. Langer, *Z. Metallkd.*, 1965, **56**, 851-852.
40. R. F. Brebrick and R. S. Allgaier, *J. Chem. Phys.*, 1960, **32**, 1826-1831.
41. I. K. Avetisov, Y. L. Kharif and P. V. Kovtunencko, *Inorganic Materials, translated from Izvestiya Akademii Nauk SSSR, Neorganicheskie Materialy*, 1987, **23**, 455-457.
42. J. C. Lin, K. C. Hsleh, R. C. Sharma and Y. A. Chang, *Bull. Alloy Phase Diagrams*, 1989, **10**, 340-347.
43. A. Ishida, S. Matsuura, M. Mizuno, Y. Sase and H. Fujiyasu, *J. Appl. Phys.*, 1988, **63**, 4572-4574.
44. D. Ravot, *J. Less-Common Met.*, 1990, **161**, 313-319.
45. M. Iida, T. Shimizu, H. Enomoto and H. Ozaki, *Jpn. J. Appl. Phys.*, 1993, **32**, 4449-4453.
46. H. Krenn, W. Herbst, H. Pascher, Y. Ueta, G. Springholz and G. Bauer, *Phys. Rev. B*, 1999, **60**, 8117-8128.
47. B. Houston, R. E. Strakna and H. S. Belson, *J. Appl. Phys.*, 1968, **39**, 3913-3916.
48. S. Yoneda, M. Kato and I. J. Ohsugi, *J. Appl. Phys.*, 2010, **107**, 074901.
49. W. Liu, Q. Jie, H. S. Kim and Z. Ren, *Acta Mater.*, 2015, **87**, 357-376.
50. Q. Zhang, H. Wang, Q. Zhang, W. Liu, B. Yu, H. Wang, D. Wang, G. Ni, G. Chen and Z. Ren, *Nano Lett.*, 2012, **12**, 2324-2330.
51. W. W. Scanlon, *Phys. Rev.*, 1962, **126**, 509-512.
52. E. H. Putley, *Proc. Phys. Soc. B*, 1955, **68**, 22-34.
53. A. V. Dmitriev and E. S. Tkacheva, *J. Electron. Mater.*, 2014, **43**, 1280-1288.
54. R. F. Brebrick and E. Gubner, *J. Chem. Phys.*, 1962, **36**, 1283-1289.
55. B. Zhang, C. Cai, S. Jin, Z. Ye, H. Wu and Z. Qi, *Appl. Phys. Lett.*, 2014, **105**, 22109.
56. S. Bajaj, G. S. Pomrehn, J. W. Doak, W. Gierlotka, H.-j. Wu, S.-W. Chen, C. Wolverton, W. A. Goddard, III and G. J. Snyder, *Acta Mater.*, 2015, **92**, 72-80.

57. L. Wun-Fan, F. Chang-Ming, D. Marjolein and A. v. H. Marijn, *J. Phys. Cond. Mat.* 2015, **27**, 355801.
58. K. Shogenji and S. Uchiyama, *J. Phys. Soc. Jap.*, 1957, **12**, 252-258.

Figures

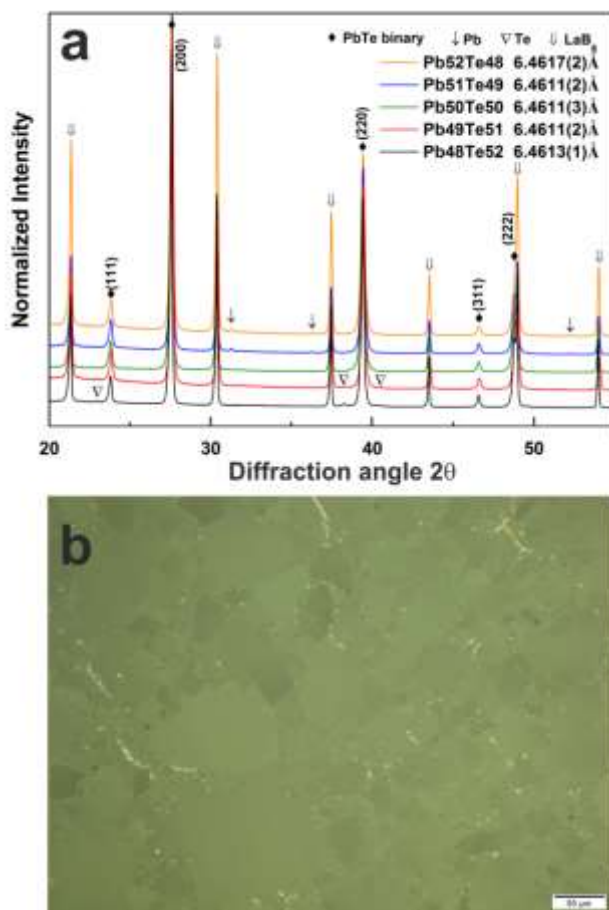


Fig.1. (a) X-ray powder diffraction patterns of binary samples $\text{Pb}_{50\pm x}\text{Te}_{50\pm x}$ revealing single-phase character for the composition $\text{Pb}_{50}\text{Te}_{50}$. (b) Microstructure (polarized light image) of the SPS-prepared sample $\text{Pb}_{50}\text{Te}_{50}$ with single-phase grains of the size $\geq 50 \mu\text{m}$; no minority phases are visible.

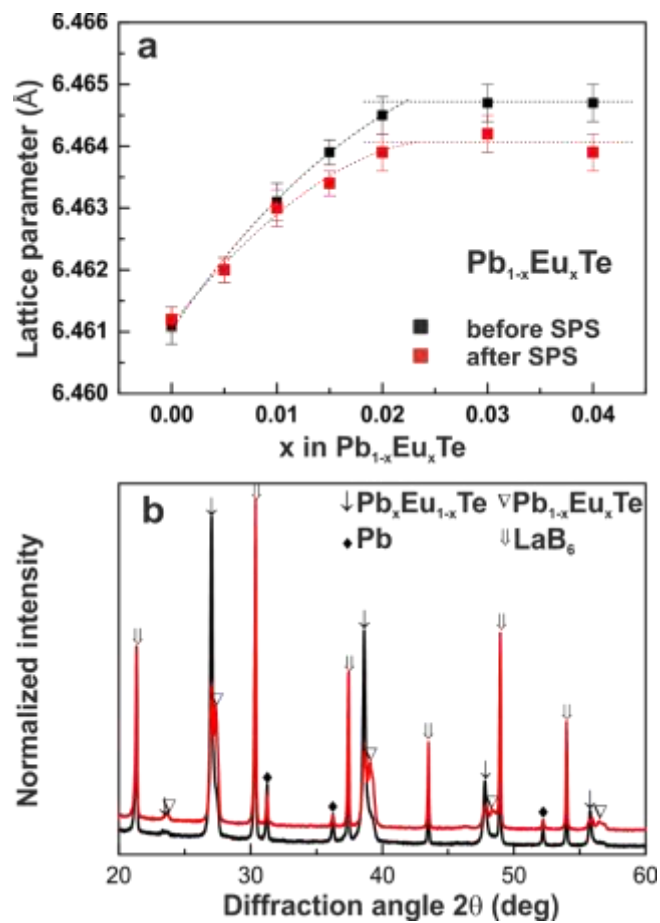


Fig. 2. (a) Lattice parameters of $Pb_{1-x}Eu_xTe$ before (black) and after (red) SPS. (b) Room-temperature X-ray diffraction pattern of $Pb_{0.50}Eu_{0.50}Te$ prepared by induction heating (red) or by technique used in Ref. 44 (black).

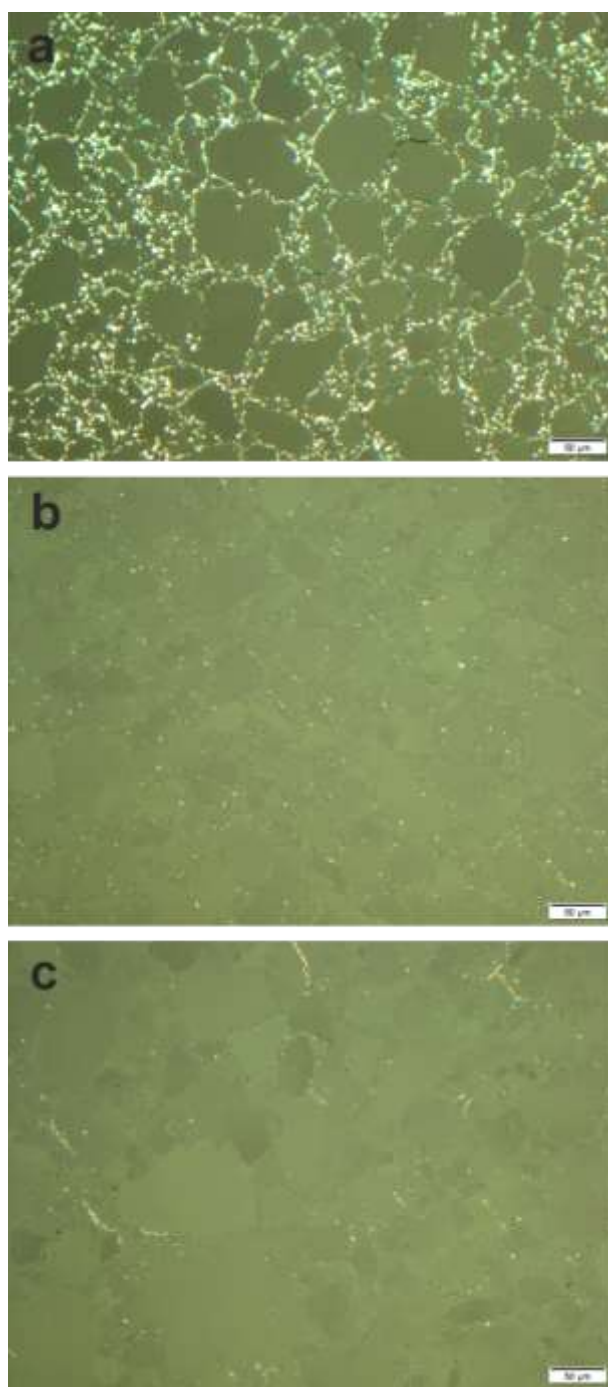


Fig. 3. Microstructure (polarized light images) of single-phase samples: $\text{Pb}_{50}\text{Te}_{50}$ after annealing at 773 K for one day (a), $\text{Pb}_{0.99}\text{Eu}_{0.01}\text{Te}$ after SPS (b) and $\text{Pb}_{0.98}\text{Eu}_{0.02}\text{Te}$ after SPS (c).

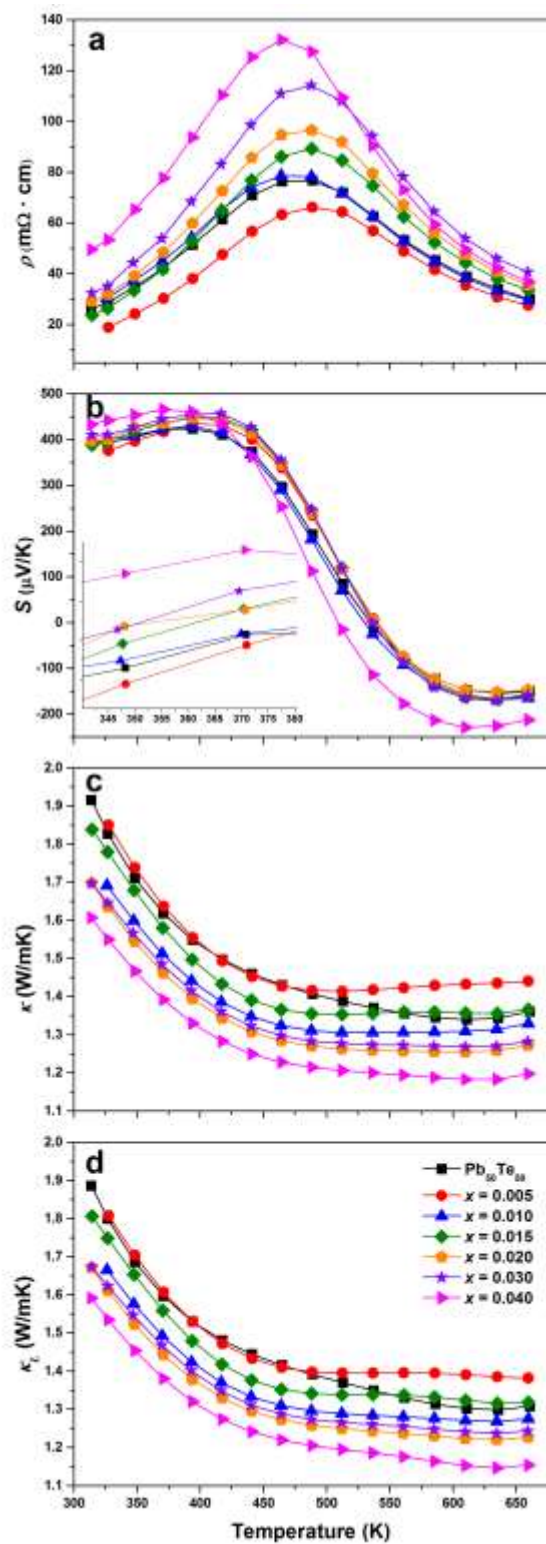


Fig. 4. Temperature dependent thermoelectric properties of $\text{Pb}_{1-x}\text{Eu}_x\text{Te}$: electrical resistivity (a), Seebeck coefficient (b), total thermal conductivity (c), lattice thermal conductivity (d).

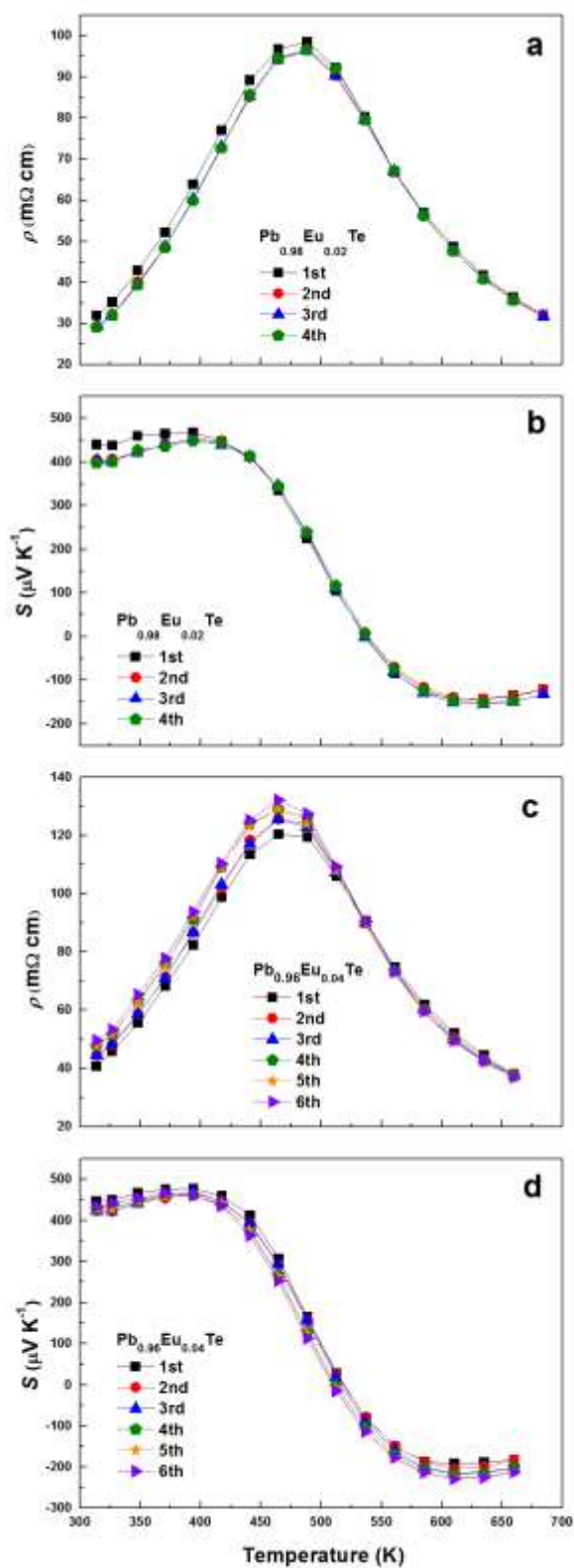


Fig. 5. Cyclic measurements of thermoelectric properties of (a, b) $\text{Pb}_{0.98}\text{Eu}_{0.02}\text{Te}$ (four cycles) and (c, d) $\text{Pb}_{0.96}\text{Eu}_{0.04}\text{Te}$ (six cycles).

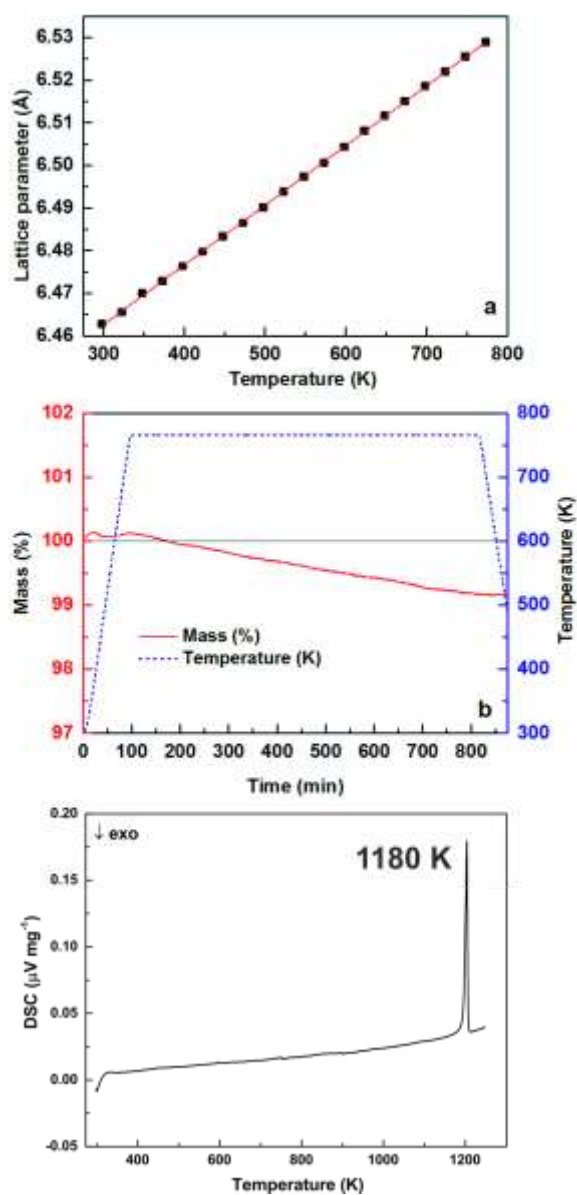


Fig. 6. Thermal behavior of the sample $\text{Pb}_{50}\text{Te}_{50}$: (a) temperature dependence of the lattice parameter; (b) thermogravimetric experiment revealing slight mass loss at 773 K; (c) DSC measurement shows only the melting point of lead telluride at 1180 K.

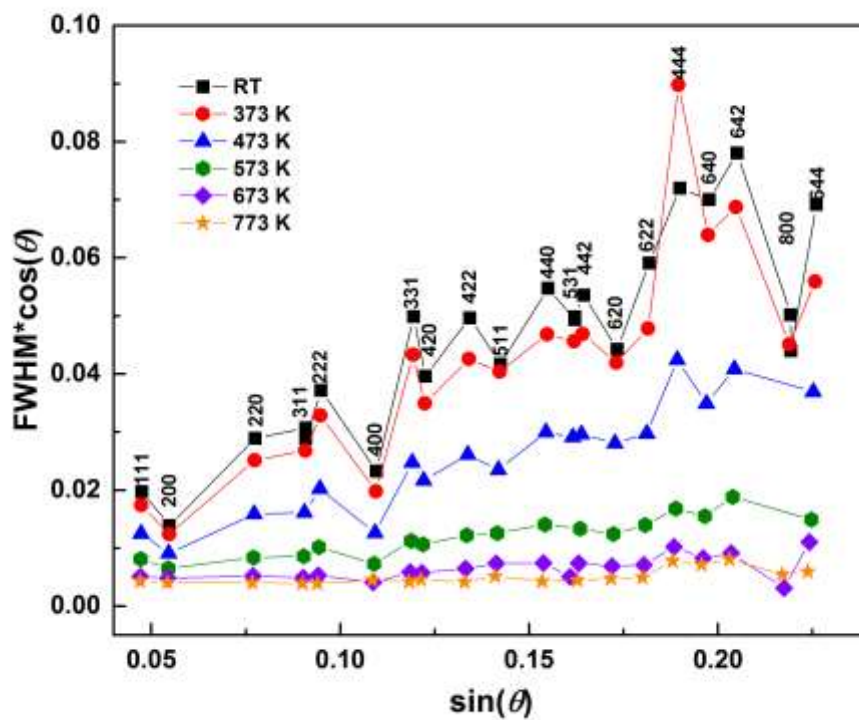


Fig. 7. Full widths at half maximum (FWHM) of the X-ray powder diffraction reflections of $\text{Pb}_{50}\text{Te}_{50}$ after SPS vs. diffraction angle at different temperatures.

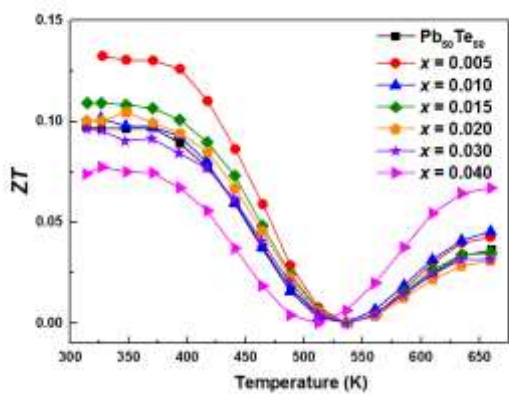


Fig. 8. Temperature dependence of the thermoelectric figure-of-merit ZT for $\text{Pb}_{1-x}\text{Eu}_x\text{Te}$.